Truncated corner cubes with near-perfect retroreflection efficiency

Eunkyong Moon,[1] Shin-Woong Park,[2] Hayun Chung,[1] Joon-Yong Lee,[3] Chanyeol Bae,[3] Jin-Woo Kim,[3] Jeongyeup Paek,[4] and Hwi Kim[1,*]

[1]ICT Convergence Technology for Health & Safety and Department of Electronics and Information Engineering, Korea University, 2511 Sejong-ro, Sejong 339-700, South Korea

[2]Center for Advanced Photovoltaic Materials, Korea University, 2511 Sejong-ro, Sejong 339-700, South Korea

[3]MNtech Co., Ltd. 16 Gwahaksaneop 1-ro, Oksan-myeon, Cheongwon-gun, Chungcheongbuk-do 363-911, South Korea

[4]Department of Computer Information Communication Engineering, Hongik University, 2639 Sejong-ro, Sejong 339-701, South Korea

*Corresponding author: hwikim@korea.ac.kr

Received 3 July 2014; revised 13 September 2014; accepted 19 October 2014; posted 21 October 2014 (Doc. ID 216323); published 18 November 2014

By isolating a finite effective volume from a conventional triangular pyramid corner cube, we obtained truncated corner cube structures with greatly enhanced retroreflection efficiency. We explore an optimal truncated corner cube with near 100% retroreflection efficiency based on the expectation that the traveling paths of the optical rays can be localized in the finite effective volume of the structure, and, as a result, truncated corner cubes with perfect efficiency can be produced. As a case study, the retroreflection efficiency of a commercialized 3M truncated corner cube sample is evaluated. Furthermore, it is shown with numerical verification that a truncated corner cube array sheet with near-perfect retroreflection efficiency can be produced. © 2014 Optical Society of America

OCIS codes: (080.2740) Geometric optical design; (120.5700) Reflection; (120.4570) Optical design of instruments.

http://dx.doi.org/10.1364/AO.53.007972

1. Introduction

Retroreflection involves the return of light back toward the optical source along the line of incidence. Retroreflection is widely used for engineering applications such as safety vests and traffic signs, and in retroreflective projection technology [1–5]. A triangular pyramid corner cube is a commonly used optical device for optical retroreflection. In many applications, retroreflection performance is evaluated in terms of retroreflection efficiency. The retroreflection efficiency is defined by the ratio of the retroreflection power to the total illumination power. For the conventional pyramid corner cube, the retroreflection efficiency can be interpreted as the areal ratio of the effective area through which an incident light ray bundle passes and is properly retroreflected to an optical source to the whole entrance facet area of the corner cube.

In principle, the retroreflection of a conventional triangular pyramid corner cube with reflecting facets is omnidirectional, but, due to limitations in retroreflection efficiency, a transparent dielectric corner cube structure based on total internal reflection is commonly used in practice. In this case, the effective retroreflection area is strongly dependent on the structural parameters and the direction of incident light. In previous studies on the optical properties of corner cube structures [6–12], it has been shown that, in theory, the maximum retroreflection efficiency of a conventional triangular pyramid corner cube is 68%.

1559-128X/14/337972-07$15.00/0

The effective retroreflection area refers to a specified region on the entrance facet of the corner cube through which incident rays can be perfectly retroreflected through triple orthogonal total internal reflections. The rays that fall outside the effective retroreflection area do not experience triple total internal reflections at perfectly orthogonal facets and thus deviate from the perfect retroreflection path. These stray rays are considered as optical loss from the performance point of view.

Given the presence of this effective retroreflection area, it is assumed that, if the finite volume within the effective area of the triangular pyramid corner cube is isolated and a truncated corner cube is produced, near-perfect (100%) retroreflection efficiency can be achieved. Furthermore, a periodic array of individual truncated corner cubes would be expected to form a perfect corner cube sheet with near 100% retroreflection efficiency. This expectation leads to the supposition that the traveling paths of the optical rays that succeed in retroreflection can be localized in the finite effective volume inside the truncated corner cube structure.

In this paper, we investigate the feasibility of a 100% efficient retroreflection corner cube and test the validity of the supposition above with ZEMAX optical modeling software. The truncated corner cube is geometrically modeled, and an estimation method for the effective retroreflection efficiency is proposed. In this study, the effect of the sidewalls of the truncated corner cube on retroreflection is given particular attention. We carry out structural optimization of the truncated corner cube structure and, as a result, present an optimal design for a truncated retroreflection corner cube with near 100% retroreflection efficiency, which supports the validity of the finite effective retroreflection volume. As a case study, the retroreflection efficiency of a commercialized truncated corner cube sheet produced by 3M Co. [13,14] is analyzed. This paper is organized as follows. In Section 2, the geometric structure of the truncated corner cube is modeled and the structure of the 3M corner cube sheet (3M Scotchlite ASTM level IX corner cube sheet) is analyzed. In Section 3, a method for estimating the effective retroreflection area of the truncated corner cube structure is described with ZEMAX, and the effective retroreflection efficiency of the 3M corner cube is numerically measured. The effective retroreflection areas of the truncated corner cube sheets are visualized in Section 4, and concluding remarks follow in Section 5.

2. Geometric Structure of a Truncated Corner Cube

In Fig. 1(a), a triangular pyramid corner cube structure is shown in the form of its local coordinate system (x, y, z), where the apex point of the corner cube is put on the origin, (0, 0, 0), and the three vertices of the entrance facet are on the x, y, and z intercepts, $(x_0, 0, 0)$, $(0, y_0, 0)$, and $(0, 0, z_0)$, respectively. The retroreflection efficiency of the triangular pyramid corner cube can be the theoretical maximum value of

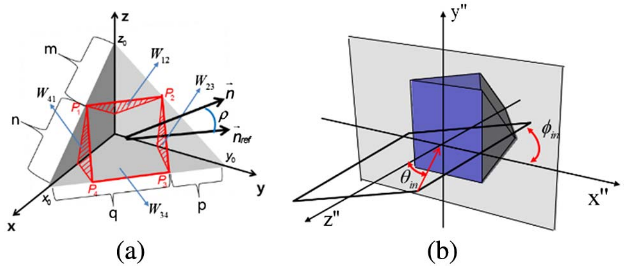

Fig. 1. (a) Construction of the truncated corner cube and (b) truncated corner cube as depicted in the global coordinate system.

68%, and the retroreflection area has a hexagon pattern [11]. The tilting angle of the triangular pyramid corner cube structure is defined by the angle of intersection of the surface normal vector and the reference vector $\mathbf{n}_{\mathrm{ref}} = (1, 1, 1)$. The surface normal of the entrance facet is $\mathbf{n} = (1/x_0, 1/y_0, 1/z_0)$. The tilt angle ρ is given by

$$\rho = \mathrm{acos}\left(\frac{1/x_0 + 1/y_0 + 1/z_0}{\sqrt{3}\sqrt{(1/x_0)^2 + (1/y_0)^2 + (1/z_0)^2}}\right). \quad (1)$$

The truncated corner cube is extracted by cutting the rectangular part in the entrance facet. The cutting direction is in the normal direction to its entrance facet as shown in Fig. 1(a). As a result, the truncated corner cube has three sidewalls, W_{12}, W_{23}, and W_{41}, which are specified by the areas shaded in red in Fig. 1(a). The normal vectors of the sidewalls are perpendicular to the entrance facet. The corner points of the entrance facet are denoted by P_1, P_2, P_3, and P_4, which are on the edges of the triangular pyramid corner cube. To maximize retroreflection efficiency, the rectangular area $P_1P_2P_3P_4$ should be covered by the hexagonal retroreflection area of the triangular pyramid corner cube.

The corner points, P_1, P_2, P_3, and P_4, are the points of internal division of the edges of the triangular entrance facet. Let the truncation ratio be $m:n$; then the points P_1, P_2, P_3, and P_4 can be represented, in terms of the intercepts, x_0, y_0, and z_0, as follows,

$$P_1 = \frac{n}{m+n}(0, 0, z_0) + \frac{m}{m+n}(x_0, 0, 0), \quad (2a)$$

$$P_2 = \frac{n}{m+n}(0, 0, z_0) + \frac{m}{m+n}(0, y_0, 0), \quad (2b)$$

$$P_3 = \frac{p}{p+q}(x_0, 0, 0) + \frac{q}{p+q}(0, y_0, 0), \quad (2c)$$

$$P_4 = P_3 + (P_1 - P_2). \quad (2d)$$

p and q are expressed in terms of $P_1 = (P_{1x}, 0, P_{1z})$ and $P_2 = (0, P_{2y}, P_{2z})$, respectively, as

$$p = \left(\sqrt{x_0^2 + y_0^2} - \sqrt{P_{1x}^2 + P_{2y}^2} \right) / 2, \tag{3a}$$

$$q = \sqrt{x_0^2 + y_0^2} - p. \tag{3b}$$

The plane equations of the sidewalls, W_{12}, W_{23}, W_{34}, and W_{41}, are obtained as

$$W_{12} : \mathbf{n}_{12} \cdot (\mathbf{r} - P_1) = 0, \tag{4a}$$

$$W_{23} : \mathbf{n}_{23} \cdot (\mathbf{r} - P_2) = 0, \tag{4b}$$

$$W_{34} : \mathbf{n}_{34} \cdot (\mathbf{r} - P_3) = 0, \tag{4c}$$

$$W_{41} : \mathbf{n}_{41} \cdot (\mathbf{r} - P_4) = 0, \tag{4d}$$

where $\mathbf{n}_{12}$, $\mathbf{n}_{23}$, $\mathbf{n}_{34}$, and $\mathbf{n}_{41}$ are the surface normals of $W_{12} W_{23} W_{34}$, and W_{41}, respectively, and given as

$$\mathbf{n}_{12} = \mathbf{n} \times (\overrightarrow{P_2 P_1}), \tag{5a}$$

$$\mathbf{n}_{23} = \mathbf{n} \times (\overrightarrow{P_3 P_2}), \tag{5b}$$

$$\mathbf{n}_{34} = \mathbf{n} \times (\overrightarrow{P_4 P_3}), \tag{5c}$$

$$\mathbf{n}_{41} = \mathbf{n} \times (\overrightarrow{P_1 P_4}). \tag{5d}$$

By changing the truncation ratio of m/n (or setting $n = 1$ and changing m), we can obtain several truncated corner cubes with different entrance facets. The truncated corner cube is presented in the global coordinate system, (x'', y'', z''), in Fig. 1(b). The incidence and azimuthal angles of an incoming ray are denoted by θ_{in} and ϕ_{in}, respectively.

Using this structure model, we carry out structural analysis of a commercialized truncated corner cube sheet produced by 3M Co. In Fig. 2, the top-view microscope image and schematics of the disassembled truncated corner cube sheet are presented with measurements for the dimensions. Figures 2(a) and 2(b) show the top view of the truncated corner cube model and the entrance facet area of the truncated corner cube structure relative to the original triangular pyramid corner cube, respectively. Since, during a practical inspection of the truncated corner cube, the cross section of the truncated corner cube is relatively easy to measure, the measured dimensions of both the top view and the cross-section view of the truncated corner cube are indicated in Figs. 2(c) and 2(d), respectively.

For an isosceles triangular pyramid corner cube with the base angle θ_1, we can set $x_0 = y_0$, and x_0/z_0 is solved as

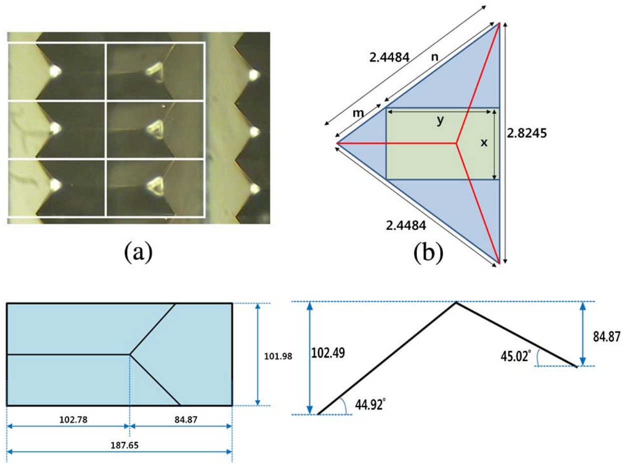

(a) (b) (c) (d)

Fig. 2. (a) Structure of the 3M truncated corner cube sheet. (b) Top view of the truncated corner cube relative to that of the triangular pyramid corner cube. (c), (d) Linear dimensions of (c) top view and (d) the cross-section view.

$$\cos\theta_1 = \frac{z_0}{\sqrt{\frac{1}{2}(x_0)^2 + (z_0)^2}} = \frac{1}{\sqrt{\frac{1}{2}(x_0/z_0)^2 + 1}}. \tag{6a}$$

For the example in Fig. 2, the measured value of the base angle θ_1 is 44.92°. From Eq. (6a), x_0/z_0 is obtained as

$$x_0/z_0 = \sqrt{2\left(\frac{1}{(\cos\theta_1)^2} - 1\right)} = 1.4103. \tag{6b}$$

Let us consider the scale-normalized structure constraint by

$$(1/x_0)^2 + (1/y_0)^2 + (1/z_0)^2 = 1; \tag{6c}$$

then the structural parameters are calculated as $x_0 = 1.9972$, $y_0 = 1.9972$, and $z_0 = 1.4162$. The tilt angle of the structure ρ is calculated from Eq. (1) to be 9.6556°. The directional vector of the incidence ray with incidence angle, θ_{in}, and azimuth angle, ϕ_{in}, is

$$(k_{ix}, k_{iy}, k_{iz}) = (\cos\phi_{in}\sin\theta_{in}, \sin\phi_{in}\sin\theta_{in}, -\cos\theta_{in}). \tag{7a}$$

The directional vector of the refracted ray in the triangular pyramid corner cube with refractive index n_c is

$$(k_{rx}, k_{ry}, k_{rz}) = (\cos\phi_r\sin\theta_r, \sin\phi_r\sin\theta_r, -\cos\theta_r). \tag{7b}$$

The refraction vector is solved by the incidence vector as

$$(\cos\phi_r \sin\theta_r, \sin\phi_r \sin\theta_r, -\cos\theta_r) = \frac{1}{n_c}\left(\cos\phi_{in}\sin\theta_{in}, \sin\phi_{in}\sin\theta_{in}, -\sqrt{n^2 - (\sin\theta_{in})^2}\right). \tag{7c}$$

For the triangular pyramid corner cube, the incidence angle of illumination that offers the maximum effective retroreflection area can be calculated by the formula developed in Ref. [11]. The ray vector of the maximum effective retroreflection is given by

$$\begin{bmatrix} \cos\phi_r \sin\theta_r \\ \sin\phi_r \sin\theta_r \\ -\cos\theta_r \end{bmatrix} = \frac{1}{\sqrt{x_0^2 + y_0^2 + z_0^2}} \mathbf{M} \begin{bmatrix} -x_0 \\ -y_0 \\ -z_0 \end{bmatrix}, \tag{8a}$$

where $\mathbf{M}$ and its components are given, respectively, by

$$\mathbf{M} = \begin{bmatrix} 0 & 1 & 0 \\ -1 & 0 & 0 \\ 0 & 0 & 1 \end{bmatrix} \times \begin{bmatrix} \cos\theta_s \cos\phi_s & \cos\theta_s \sin\phi_s & -\sin\theta_s \\ -\sin\phi_s & \cos\phi_s & 0 \\ \sin\theta_s \cos\phi_s & \sin\theta_s \sin\phi_s & \cos\theta_s \end{bmatrix}, \tag{8b}$$

$$\cos\theta_s = 1/z_0 = 0.7061, \tag{8c}$$

$$\sin\theta_s = \sqrt{(1/x_0)^2 + (1/y_o)^2} = 0.7081, \tag{8d}$$

$$\cos\phi_s = (1/x_0)/\sin\theta_s = 0.7071, \tag{8e}$$

$$\sin\phi_s = (1/y_0)/\sin\theta_s = 0.7071. \tag{8f}$$

From Eq. (8a), $\cos\theta_r$, $\sin\theta_r$, $\cos\phi_r$, and $\sin\phi_r$ are obtained as 0.9495, 0.3138, 0, and 1, respectively. For a refractive index of $n_c = 1.55$ (conventional glass, NBK7 in ZEMAX), the optimal incident and azimuthal angles for the maximum effective retroreflection area are estimated to be, respectively, from Eq. (7c),

$$\theta_{in} = \mathrm{asin}(n \sin\theta_r) = 29.1078 \text{ (deg)}, \tag{8g}$$

$$\phi_{in} = 90 \text{ (deg)}. \tag{8h}$$

In Fig. 2(b), the horizontal and vertical sizes of the truncated corner cube are represented by $x = 2.8245m/(m+n)$ and $y = 2.0n/(m+n)$, respectively. From the measured ratio, we obtain the equation

$$x(101.98){:}y(172.45) = 2.8245m{:}2.0n. \tag{9}$$

Consequently, we have obtained the truncation ratio, $m/n = 0.385$.

3. Estimation of the Effective Retroreflection Area

In general, the effective retroreflection area of a triangular pyramid corner cube varies according to the direction of illumination. Thus, by changing the tilt angle of the corner cube, we can design an optimal corner cube structure with a theoretical maximum retroreflection efficiency of 68% for any given illumination direction.

It is expected that a truncated corner cube will have near 100% retroreflection efficiency. However, to achieve this goal, the traveling paths of the optical rays that undergo successful retroreflection should be localized in the finite effective volume inside the corner cube structure and thus not affected by the truncation. In this section, the effective retroreflection areas of the truncated corner cubes are analyzed, and, as a consequence, it is demonstrated that near-perfect retroreflection can be achieved with a truncated corner cube.

As defined in Section 2, the entrance facet of a truncated corner cube varies with design factors such as the truncation ratio m/n and the tilt angle ρ. For a triangular pyramid corner cube, retroreflection occurs when the ray is reflected three times at the orthogonal facets of the perfect corner cube. If the necessary condition of triple orthogonal reflections inside the structure is not satisfied, rays cannot be accurately retroreflected, and they become stray rays. Similarly, the sidewalls of a truncated corner cube can also generate stray rays; however, the paths of these rays are more complicated than those of the triangular pyramid corner cube. Estimation of the effective retroreflection area is not easy due to the interference and mixing of stray rays; therefore, the separation of the target retroreflected rays from any stray rays is necessary.

The simulation setup in ZEMAX for the analysis of the truncated corner cube is shown in Fig 3. The truncated corner cube is placed on the optical axis. A point light source is placed a distance away from the truncated corner cube. The rays emitted from the light source were tuned to diverge slightly to

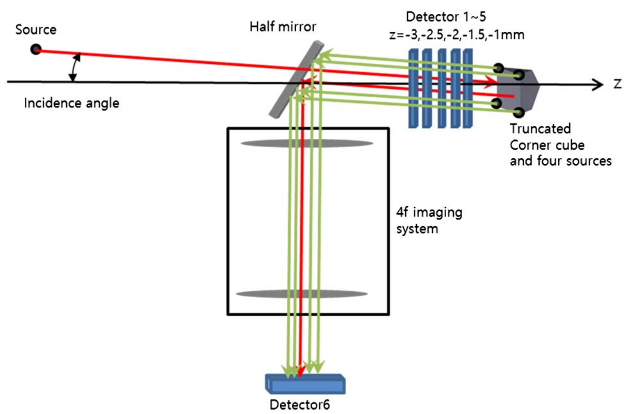

Fig. 3. ZEMAX simulation setup for the analysis of the retroreflection of a truncated corner cube. The 4-f system is composed of two thin lenses with focal length 1100 mm, and Detector 6 is located at a distance of 4400 mm from the truncated corner cube.

cover the entrance facet of the truncated corner cube for efficient simulation. Since the truncated corner cube is dielectric, both reflection and transmission take place, but only reflected rays require measurement. As mentioned, the reflected rays are a mixture of retroreflected and stray rays. Therefore, a 4-f imaging system [15] is installed to filter out the stray components and accurately measure the effective retroreflection area as shown in Fig. 3. When the rays from the point source meet the truncated corner cube, the reflected rays travel in the reverse direction of incidence. On their path to the optical detectors, a half-mirror guides those reflected rays to pass through the 4-f imaging system. During propagation, the stray rays with nonparaxial directions are rejected via the vignetting effect. The optical intensity distribution taken in Detector 6 is equivalent to the effective retroreflection area of the truncated corner cube without stray light interference.

In the analysis, the stray rays are measured sequentially using five unidirectional detectors numbered from 1 to 5 and located with 0.5 mm intervals starting from 1 mm in front of the truncated corner cube, enabling the propagation of stray rays to be monitored. Figure 4 shows the simulation results for the stray light. In this simulation, the truncation ratio and the incidence angle are set to $m/n = 1.3$ and 25°, respectively. The optical intensity distributions measured by Detectors 1–5 are presented in Figs. 4(a)–4(e), respectively. The entrance facet area is indicated by the white rectangle. Inspecting Figs. 4(a)–4(e), two distinguished light components are observed. One is a light pattern that does not vary with detector position, and the other is a light pattern that varies widely. These two patterns are considered the retroreflected and stray light components, respectively. We succeed in the selective imaging of the retroreflection effective area by filtering out the stray rays generated by the sidewalls of the truncated corner cube. The light distribution obtained through the 4-f system is shown in Fig. 4(f). The 4-f system shown in Fig. 3 filters the stray light and selectively images the effective retroreflection area on Detector 6. The effective retroreflection area is extended within the entrance facet aperture, but does not seem to completely fill the aperture. In this case, the effective retroreflection efficiency, RA, is estimated to be RA = 71.51%. As can be seen in Fig. 4, the simulation setup of Fig. 3 offers an analysis tool for the effective retroreflection area of truncated corner cubes.

Following this, a number of other truncated corner cubes require testing in order to find an optimal structure with near 100% retroreflection efficiency. Sixteen models are prepared with different truncation ratios that vary from $m/n = 0.1$ to $m/n = 1.6$, with a variation interval of $\Delta(m/n) = 0.1$. Figures 5(a)–5(p) present the measured effective retroreflection areas of these structures.

The incidence angle of illumination is set to 4°, and the tilt angle of the corner cube ρ is set to 2.286°. When m increases beyond $m/n = 1.6$, the intersection point for W_{12} and the z axis crosses the origin point. Thus, in the analysis, m is limited to 1.6. As a consequence, from the results displayed in Fig. 5, the effective retroreflection efficiency that is closest to 100% occurs when the ratio m/n is 0.4.

For a given triangular pyramid corner cube with a specified tilt angle ρ, the retroreflection efficiency of

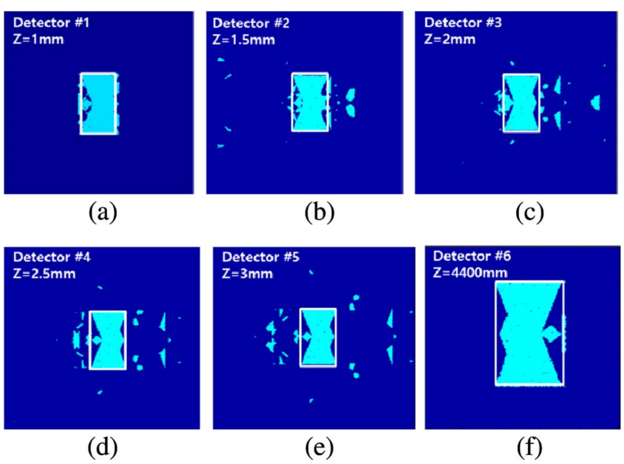

Fig. 4. Optical intensity patterns of the reflected rays generated by oblique illumination with incidence angle 25° on a truncated corner cube with the truncation ratio $m/n = 1.3$. (d)–(f) Optical intensity patterns observed at the detector planes: (a) Detector 1; (b) Detector 2; (c) Detector 3; (d) Detector 4; (e) Detector 5; and (f) Detector 6.

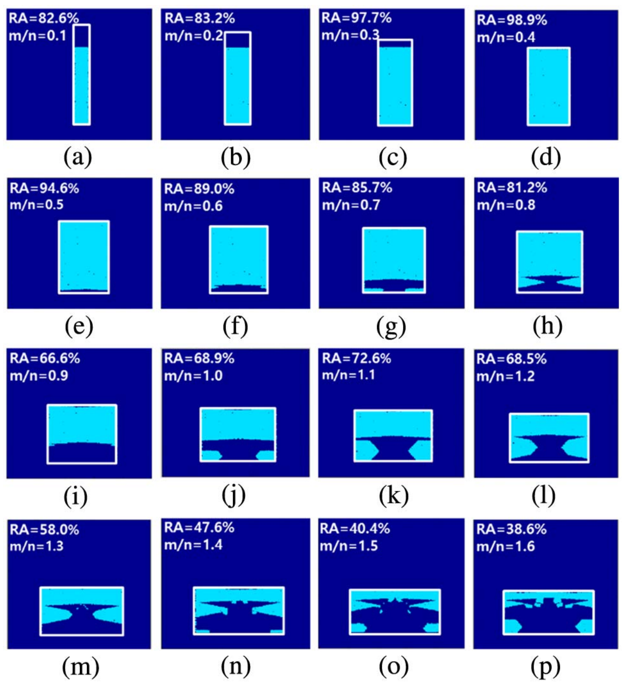

Fig. 5. Effective retroreflection areas of the truncated corner cubes with various truncation ratios: (a) $m/n = 0.1$; (b) $m/n = 0.2$; (c) $m/n = 0.3$; (d) $m/n = 0.4$; (e) $m/n = 0.5$; (f) $m/n = 0.6$; (g) $m/n = 0.7$; (h) $m/n = 0.8$; (i) $m/n = 0.9$; (j) $m/n = 1.0$; (k) $m/n = 1.1$; (l) $m/n = 1.2$; (m) $m/n = 1.3$; (n) $m/n = 1.4$; (o) $m/n = 1.5$; and (p) $m/n = 1.6$.

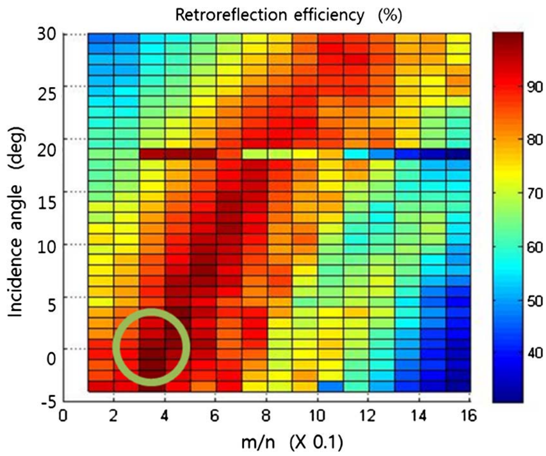

Fig. 6. Effective retroreflection efficiency variation for incidence angle and truncation ratio.

the truncated corner cube can vary with incidence angle and truncation ratio. Figure 6 plots the effective retroreflection efficiency as a function of the incidence angle and the truncation ratio with the same structure as analyzed in Fig. 5. The incidence angle and the truncation ratio are scanned from −4° to 30° and from 0.1 to 1.6, respectively, to find the conditions of the highest effective retroreflection efficiency. From this, it is shown that an effective retroreflection efficiency of 99.7% is achieved at the ratio of m/n 0.3 and an incidence angle of −2°.

In addition, the effective retroreflection efficiency of the truncated corner cube structure produced by 3M Co. that is analyzed in Section 2 is analyzed here using the devised analysis setup. Variation in retroreflection efficiency according to incidence angle is plotted in Fig. 7. The retroreflection efficiency of the truncated corner cube is analyzed for incidence angles from −88° to 88°. The maximum retroreflection efficiency, 97.57%, is observed at an incidence angle of 0°, i.e., normal incidence. The graph shows the sharp variation in retroreflection efficiency around this optimal point.

The tolerance of the incidence angle around the normal incidence seems to be relatively small. It is also furthermore noteworthy that the optimal incidence angle for the truncated corner cube is 0° compared to the optimal incidence angle of the triangular pyramid corner cube of about 29.11° [see Eq. (8g)]. The truncation operation thus changes the optimal incidence angle.

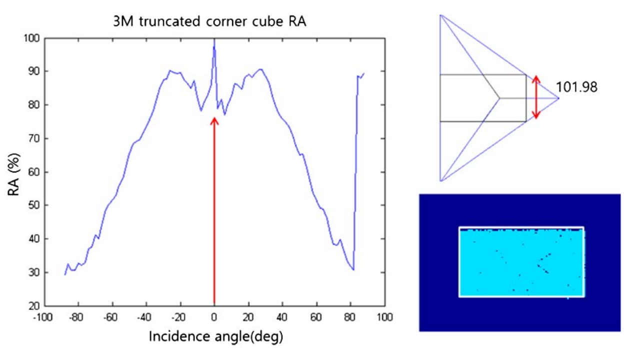

Fig. 7. Analysis of retroreflection efficiency of the 3M truncated corner cube structure with tilt angle = 9.6556° and truncation ratio $m/n = 0.385$. The highest retroreflection efficiency (RA%) is obtained at the incidence angle of 0°.

4. Retroreflection of Truncated Corner Cube Sheets

In practice, identical truncated corner cubes are arranged to a sheet as an array [16–20]. It would be expected that optical interference across the interfaces of adjacent truncated corner cubes could change the effective retroreflection area of each individual truncated corner cube.

To check whether the arrangement influences the retroreflection efficiency of an individual truncated corner cube in the sheet to be reduced from that of the single unit truncated corner cube, we perform ZEMAX simulation of 10 × 10 arrays for two different truncated corner cube structures with $m/n = 0.4$ and $m/n = 1$. The original triangular pyramid corner cube from which the truncated corner cubes are formed has a tilt angle of 2.286°, which is identical to the structure analyzed in Fig. 5. The effective retroreflection areas of the truncated corner cube sheets are presented in Figs. 8(c) and 8(f) for comparison. The first sheet structure shows an effective retroreflection efficiency of about 98.9%, meaning that most of its incidence area contributes to retroreflection. In other words, retroreflection efficiency is preserved even within an array formation. The effective area

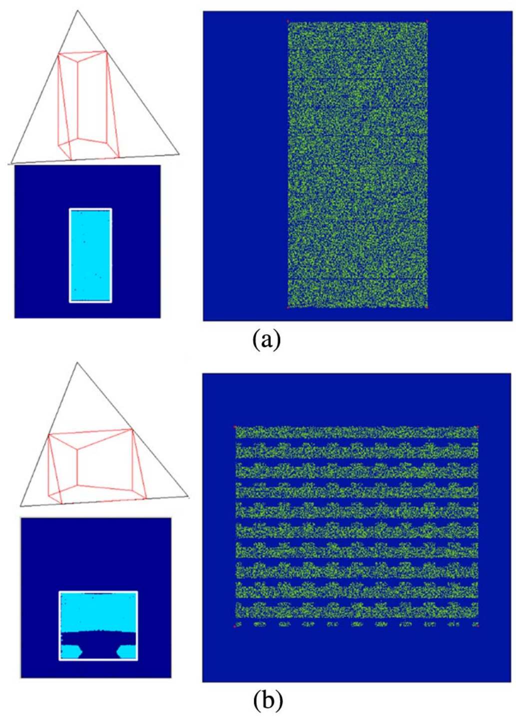

Fig. 8. Effective retroreflection areas of the corner cube sheets with (a) optimal units ($m/n = 0.4$) and (b) nonoptimal units ($m/n = 1$). The left column shows the perspective view of the truncated corner cube and its effective retroreflective area. In the right column, the effective retroreflective areas of the sheets are presented.

of the truncated corner cube sheet with the truncation ratio $m/n = 1$ is shown in Fig. 8(f). The array, which consists of individual truncated corner cubes with 68.9% efficiency, offers a 10×10 periodic pattern of the same retroreflection efficiency. The analysis confirms that the periodic arrangement of truncated corner cubes into arrays preserves the near-perfect retroreflection property of a single truncated corner cube unit. In the periodic arrangement; inter-unit interference does not affect the total retroreflection properties. It supports our argument that the internal ray paths for retroreflection are localized in a finite volume for each truncated corner cube structure.

5. Conclusion

In conclusion, we have investigated the retroreflection characteristics of truncated corner cubes with geometrical analysis and ZEMAX simulation and presented an optimal truncated corner cube structure with near-perfect retroreflection efficiency. It is revealed that the selected commercial truncated corner cube has near-perfect retroreflection efficiency at normal incidence. It is inferred that the near-perfect retroreflection efficiency is due to the localization properties of the internal ray paths within the truncated corner cube. Truncated corner cube structures with near-perfect retroreflection efficiency can be used for high-performance premium optical sheet products for traffic signage and safety applications as well as various engineering applications.

This work was supported by a Korean University grant.

References

1. H. Yamamoto and S. Suyama, "Aerial 3D LED display by use of retroreflective sheeting," Proc. SPIE **8648**, 86480Q (2013).
2. T. Yoshida, K. Shimizu, T. Kurogi, S. Kamuro, K. Minamizawa, H. Nii, and S. Tachi, "RePro3D: full-parallax 3D display with haptic feedback using retro-reflective projection technology," in *IEEE International Symposium on VR Innovation* (IEEE, 2011), pp. 49–54.
3. J. Fergason, "Optical system for head mounted display using retroreflector and method of displaying an image," U.S. patent 5,621,572 (15 April 1997).
4. H. Hua, A. Girardot, C. Gao, and J. P. Rolland, "Engineering of head-mounted projective displays," Appl. Opt. **39**, 3814–3824 (2000).
5. A. L. Mieremet, R. M. A. Schleijpen, and P. N. Pouchelle, "Modeling the detection of optical sights using retro-reflection," Proc. SPIE **6950**, 69500E (2008).
6. R. B. Nilsen and X. J. Lu, "Retroreflection technology," Proc. SPIE **5616**, 47–60 (2004).
7. CIE54.202001, "*Retroreflection: definition and measurement*" (Commission International de L'Eclairage, 2001).
8. H. Kim, S.-W. Min, and B. Lee, "Geometrical optic analysis of structural imperfection of retroreflection corner-cubes with nonlinear conjugate gradient method," Appl. Opt. **47**, 6453–6469 (2008).
9. M. S. Scholl, "Ray trace through a corner-cube retroreflector with complex reflection coefficients," J. Opt. Soc. Am. A **12**, 1589–1592 (1995).
10. H. Kim and B. Lee, "Geometric optics analysis of light transmission and reflection characteristics of metallic prism sheets," Opt. Eng. **45**, 084004 (2006).
11. H. Kim, S.-W. Min, and B. Lee, "Optimal design of retroreflection corner-cube sheets by geometric optics analysis," Opt. Eng. **46**, 094002 (2007).
12. D. C. O'Brien, G. E. Faulkner, and D. J. Edwards, "Optical properties of a retroreflecting sheet," Appl. Opt. **38**, 4137–4144 (1999).
13. S. K. Nestegard, G. M. Benson, C. M. Frey, J. C. Kelliher, J. E. Lasch, K. L. Smith, and T. J. Szczech, "Dual orientation retroreflective sheeting," U.S. patent 5,936,770 (10 August 1999).
14. K. L. Smith and G. M. Benson, "Raised zone retroreflective cube corner article," U.S. patent 6,136,416 (24 October 2000).
15. J. Goodman, *Introduction to Fourier Optics*, 2nd ed. (McGraw-Hill, 1996).
16. R. A. Chipman, J. Shamir, H. J. Caulfield, and Q. Zhou, "Wavefront correcting properties of corner-cube arrays," Appl. Opt. **27**, 3203–3209 (1988).
17. J. Nelson and D. Reed, "Retro-reflective sheeting with a corner cube surface pattern having angular corner cube circular regions," U.S. patent D665,584 (21 August 2012).
18. T. L. Hoopman, "Cube-corner retroreflective articles having wide angularity in multiple viewing planes," U.S. patent 4,588,258 (13 May 1986).
19. I. Mimura, "Cube corner type retroreflection article," U.S. patent 8,201,953 (19 June 2012).
20. E. Brinksmeier, R. Gläbe, and L. Schönemann, "Diamond micro chiseling of large-scale retroreflective arrays," Precis. Eng. **36**, 650–657 (2012).